N95-27643

MOLECULAR BEAM SCATTERING FROM ^{13}C-ENRICHED KAPTON AND CORRELATION WITH THE EOIM-3 CAROUSEL EXPERIMENT

Timothy K. Minton
Jet Propulsion Laboratory
Mail Stop 67-201
4800 Oak Grove Dr.
Pasadena, CA 91109
Phone: 818/354-8580, FAX: 818/393-6869

Teresa A. Moore
Division of Chemistry and Chemical Engineering
California Institute of Technology
Pasadena, CA 91125
Phone: 818/354-6128, FAX: 818/393-6869

SUMMARY

Mass spectra of products emerging from identical samples of a ^{13}C-enriched polyimide polymer (chemically equivalent to Kapton) under atomic oxygen bombardment in space and in the laboratory were collected. Reaction products unambiguously detected in space were ^{13}CO, NO, $^{12}CO_2$, and $^{13}CO_2$. These reaction products and two others, H_2O and ^{12}CO, were detected in the laboratory, along with inelastically scattered atomic and molecular oxygen. Qualitative agreement was seen in the mass spectra taken in space and in the laboratory; the agreement may be improved by reducing the fraction of O_2 in the laboratory molecular beam. Both laboratory and space data indicated that CO and CO_2 products come preferentially from reaction with the imide component of the polymer chain, raising the possibility that the ether component may degrade in part by the "evaporation" of higher molecular weight fragments. Laboratory time-of-flight distributions showed 1) incomplete energy accommodation of impinging O and O_2 species that do not react with the surface and 2) both hyperthermal and thermal CO and CO_2 products, suggesting two distinct reaction mechanisms with the surface.

INTRODUCTION

Recently, a protocol[1] has been written with the objective of providing "guidelines for materials testing in ground-based atomic oxygen environments for the purpose of predicting the durability of the tested materials in low Earth orbit (LEO)." The validity of testing under this protocol, or any other set of criteria, rests on the proven ability of the ground-based test facility to produce results that can be related in a straightforward manner to atomic-oxygen-induced effects on

materials in LEO. Both space- and ground-based studies on identical materials are required to evaluate ground-based test methods aimed at predicting materials durability in space. Such a ground-space correlation study, which involved materials exposure on the EOIM-3 flight experiment, has been reported.[2]

Proven agreement between laboratory and space experiments also adds value to the results of scientific experiments in the laboratory. It is much easier to perform sophisticated experiments in the laboratory than in space. Laboratory experiments therefore have the potential to reveal more information than space experiments about the interaction mechanisms of hyperthermal oxygen atoms with materials in LEO. The extent to which the laboratory results can lead to inferences about O-atom interactions in LEO depends on the ability of the laboratory experiment to predict effects seen in the actual LEO environment.

The EOIM-3 carousel experiment provided an ideal "calibration point" for powerful molecular beam/surface scattering experiments that can be conducted at the Jet Propulsion Laboratory (JPL). This report contains new data, both from EOIM-3 and from our laboratory at JPL, on the interaction of hyperthermal O atoms with an isotopically-labeled, Kapton-like polyimide surface. The molecular beam experiment provides the capability to examine the identity of products that emerge from the surface, as well as their directions and velocities. These diagnostic capabilities permit the interaction dynamics of fast O atoms with a surface to be inferred. The EOIM-3 carousel experiment yields information only on the identity of the scattered species; nevertheless, this information provides a common point of reference for assessing the value of the laboratory results. The new laboratory results agree qualitatively with the space observations and point the way to a clearer understanding of O-atom interactions with materials in LEO.

EXPERIMENTS

Reactive Scattering in Space

A key active experiment on EOIM-3 was the carousel experiment. This experiment has been described in detail in other papers in this session and will be briefly reiterated here with emphasis on the JPL role in the experiment. Five different materials were mounted on a carousel such that the surface normal of each material was 45° with respect to the direction of O-atom attack during exposure to atomic oxygen. The carousel could be rotated to place an individual material in view of a mass spectrometer detector whose nominal viewing axis was 90° with respect to the direction of O-atom impingement. One goal of the carousel experiment was to study the mass spectra of reactive products emerging from the surfaces and use the identity of the volatile products to help infer the reaction mechanisms of fast O atoms in space with the various surfaces. A cover was rotated over the viewed material part of the time to allow for the observation of the differences between the effect of direct O-atom attack and that of scattered O atoms.

JPL supplied one of the carousel materials, a ^{13}C-enriched polyimide polymer that is chemically equivalent to Kapton HN, which is manufactured by E. I. DuPont de Nemours and Co., Inc. ^{13}C-enrichment permits the observation of carbon monoxide (CO) reactive product, which would otherwise be obscured by the high background at a mass-to-charge ratio (*m/z*) of 28 due to molecular nitrogen in the residual atmosphere in LEO. In addition, detection of ^{13}CO and $^{13}CO_2$ proves unambiguously that products of the reaction of the impinging O atoms with the ^{13}C-enriched polyimide are being observed.

Because the ^{13}C-enriched polyimide is chemically equivalent to Kapton, we will henceforth refer to it as ^{13}C-enriched Kapton. Figure 1 illustrates the key steps in the synthesis of ^{13}C-enriched Kapton. All the carbons in one precursor, the ether, were carbon-13. Thus, the resulting polyimide film had in its repeat unit a biphenyl ether block containing twelve carbon atoms that were isotopically labeled as ^{13}C and an imide block containing ten unlabeled carbon atoms.

Figure 2 shows representative mass spectra taken with the mass spectrometer viewing the ^{13}C-enriched Kapton sample when the cover was off and when the cover was on. These data indicate that the net mass spectrum for direct reaction of O atoms with ^{13}C-enriched Kapton cannot be obtained simply by subtracting the cover-on spectrum from the cover-off spectrum. Even when the cover is on, a small peak from $^{13}CO_2$ can be seen; therefore, scattered O atoms must be reacting with the sample. If the cover were off, some of these reactions might not occur. Without substantial modeling of O-atom inelastic scattering from various surfaces on the EOIM-3 tray, it is difficult to know exactly how to represent the space data. The true mass spectrum for direct O-atom attack probably lies somewhere between the cover-off spectrum and the spectrum that is the difference of cover on and cover off.

Reactive Scattering in the Laboratory

We have initiated a study of the reaction of hyperthermal O atoms with a Kapton surface in the laboratory with the use of a crossed molecular beams apparatus.[3,4] This apparatus (see Fig. 3) allows beam/surface scattering experiments similar to the EOIM-3 carousel experiment, but it is much more powerful because it permits determination of the velocities and directions of scattered products that emerge from a surface. The atomic oxygen beam source is basically a copy of the source designed by Physical Sciences, Inc. (PSI),[5] where CO_2 laser detonation of oxygen gas is used to produce a pulsed beam of fast O atoms with translational energies near 5 eV. Our source utilizes a home-built piezoelectric pulsed molecular beam valve[6] to inject O_2 gas into the conical nozzle and a 5 J/pulse Alltec CO_2 laser to induce breakdown in the gas. The pulse repetition rate of the source was 1.8 Hz. For the scattering experiments described herein, the central portion of the hyperthermal beam was selected with a 3 mm dia. aperture (or "skimmer"), placed 80 cm from the apex of the conical nozzle, and allowed to impinge on a target, 92 cm from the apex of the nozzle, that was mounted on the end of a manipulator. Based on Kapton erosion measurements, we estimate the atomic oxygen flux at the target to be on the order of 10^{14} atoms/cm^2/pulse. A quadrupole mass spectrometer with a triply differentially pumped ionizer can be rotated about the interaction zone on the surface and can detect inelastically and reactively scattered products that

emerge from the surface in a particular direction. The distance from the surface to the ionizer of the detector is 34.5 cm, and the detector viewing angle is 3°. The mass spectrometer has been carefully designed with apertures that permit any products entering the ionizer to pass through into another differentially-pumped region. The probability of species, which pass through without being ionized, scattering back into the ionizer is therefore extremely low. Thus, measurements of the time-of-flight (TOF) distributions of species entering the detector give a true reflection of their kinetic energies. The target can be lowered out of the beam and the detector can be positioned directly along the beam axis in order to characterize the O-atom beam. When viewing the beam directly, a very small .12 mm diameter aperture is used on the front of the detector to prevent gas buildup in the ionization region.

Two samples of Kapton film, one ^{13}C-enriched and the other DuPont Kapton HN, were mounted on the end of the manipulator such that either sample could be placed in the beam path without breaking vacuum. The temperature of the sample mount was maintained at 340 K. Although the pressure in the source chamber rose to $\sim 5\times10^{-4}$ Torr during the pulse, the pressure in the main scattering chamber remained $\leq 2\times10^{-7}$ Torr during the entire experiment. The source chamber was evacuated with a 10" Varian VHS-10 oil diffusion pump, which had a water baffle that was cooled with a refrigerated liquid to 250 K. The main scattering chamber was evacuated with two 10" CTI-10 cryopumps and a liquid nitrogen cryopanel that covered the bottom of the chamber. Even with cryopumping of the main chamber and scrupulous cleaning of the samples with ultraclean ethanol prior to mounting in the chamber, a contamination layer accumulated on the samples. Although some contamination was probably being deposited constantly during exposure and thus erosion of the surface, a steady-state condition could be reached where we were certain that we were observing products of a reaction with the actual sample material and not a contamination layer on it. As will be seen below, the use of a ^{13}C-labeled sample proved that a reaction was occurring with the material. Two different means were used to rid the sample of contamination and reach steady state, as determined by observation of reactive TOF signals at CO and CO_2 product masses. One method was simply to expose the target to oxygen atoms for a long time, >10,000 pulses. To reach steady state faster, we exposed the surface to a beam of 20 keV electrons during O-atom exposure. The electron gun was oriented such that the electron beam was roughly normal to the target surface when the O-atom beam incident angle was 45°. We found that about 5 minutes of electron exposure at fluxes between 1 and 10 $\mu A/cm^2$ cleaned the surface sufficiently that subsequent reactive signals were identical to those seen after more than 10,000 pulses of the atomic oxygen beam alone. Because both methods led to identical reactive signals, it appeared that the short electron exposure did not alter the chemical reactions occurring at the surface. All the laboratory data presented in this report were collected after "cleaning" the surface with the electron beam.

Figure 4 shows TOF spectra collected with the mass spectrometer directly viewing the beam. Time zero is when the pulsed valve is triggered to open. At this time, oxygen gas begins to enter the conical nozzle. The spike about 250 μs later corresponds to the firing of the CO_2 laser. This can be considered the actual time zero for the formation of the hyperthermal beam pulse. The spike comes from photoelectrons produced in the detector by ultraviolet light emanating from the laser-induced plasma. The pulse of hyperthermal species arrives at the detector around 200 μs after the laser fires. Thermal O_2, which is not processed by the laser, takes more than 2 ms to travel 126.5 cm to the ionizer. These and all TOF distributions presented here include the ion flight time, which

is the time required for an ion to travel from the ionizer to the Daly-type ion counter. The ion flight time for a singly-charged ion of mass m has been found experimentally, and it can be expressed in μs by the formula $\alpha(m)^{1/2}$ where the parameter α is a function of ion energy and other mass spectrometer parameters and is equal to 2.24.

It can be seen from Fig. 4 that the fast species in the beam consist of both atomic and molecular oxygen. In fact, for the set of experiments discussed in this report, the O_2 content was roughly twice the O-atom content. The relative O-atom content in the hyperthermal beam pulse is very sensitive to the actual operating conditions of the source. We have observed O-atom fractions from 25-70% in beams produced in our laboratory. The ion content in a similar beam has been measured at PSI to be about 1%, which should be considered an upper limit for our beam. With the ionizer off, there is a tiny signal at m/z = 16 (or 32) whose integral is more than three orders of magnitude lower than the signal with the ionizer on. Given that the detection efficiency should be approximately four orders of magnitude higher for ions, the ion fraction in the beam is probably much less than 1%.

Because we measure the arrival time and mass of species that travel a known distance from the source to the ionizer, we can derive the energy distribution of the species in the beam pulse (assuming that the width in the measured TOF distributions is determined by particles traveling at different velocities with a single point of origin in the nozzle cone). We need only take into account the fact that the mass spectrometer is a number density detector while the translational energy distribution is proportional to flux. We thus use the relationship $P(E) \propto t^2N(t)$. Figure 5 shows the translational energy distribution of the O-atoms in the beam and the fit this distribution gives to the beam TOF distribution. The average energy of this beam was 4.7 eV, and its width (FWHM) was 2.5 eV. Figure 6 shows the analogous energy distribution and fit for the O_2 molecules in the beam. The O_2 component had a much higher average energy (8.7 eV) and energy spread (5.5 eV) than the O-atom component.

The hyperthermal beam, just described, was directed at Kapton and ^{13}C-enriched Kapton surfaces, and scattered products were monitored with the mass spectrometer detector. The angle of incidence was 45° with respect to the surface normal, and the detector axis was also 45°. Thus, the total included scattering angle was 90°, similar to the EOIM-3 carousel experiment. The beam pulse provided the timing for the experiment; no additional chopping was used. TOF distributions of scattered products were collected at m/z = 16(O^+), 18(H_2O^+), 28($^{12}CO^+$), 29($^{13}CO^+$), 30(NO^+), 32(O_2^+), 44($^{12}CO_2$), and 45($^{13}CO_2$). Typical accumulation times for each TOF distribution were 1200 beam pulses. The time resolution was limited by our multichannel scaler to 2 μs/channel. All data were collected before a total O-atom fluence of 2×10^{18} atoms/cm^2 was accumulated on either surface, so the familiar "shag-carpet" morphology was not fully developed.

LABORATORY SCATTERING RESULTS

TOF distributions for O and O_2 scattering from the ^{13}C-enriched surface are shown in Figure 7. Time zero in these distributions corresponds to the firing of the laser, so the observed arrival

time includes the flight time of the beam pulse to the surface and the flight time of scattered products from the surface to the detector. For reference, the respective beam TOF distributions are shown (dashed lines) to illustrate the slowing of the impinging species as a result of energy transfer at the surface. While the O-atom distribution is the result of inelastic scattering from the surface, the O_2 TOF distribution may have an additional contribution from O-atom recombination at the surface. It is difficult to quantify the amount of O-atom recombination without a careful study of the distributions of the scattered molecular and atomic oxygen as a function of exit angle. Nevertheless, the O_2 (and O) exhibits a behavior that is typical for inelastic scattering of energetic species from a surface.[7-11]

Regardless of whether O-atoms or O_2 molecules scatter from the surface, we see two components in the TOF distribution -- a hyperthermal component and a roughly thermal component. These two components can be understood in terms of two limiting cases of inelastic scattering.[7-11] The first is direct inelastic scattering, where an incoming atom or molecule bounces off the surface after a single collision. In this case, the interaction is too fast to allow for thermal equilibration with the surface and only a fraction of the initial kinetic energy is lost to the surface. The second case is trapping desorption, where the incoming atom or molecule becomes trapped long enough to come into thermal equilibrium with the surface and later desorbs at thermal energies. Both TOF distributions show a large direct inelastic component, demonstrating clearly that much of the initial energy is not accommodated on the surface. In these particular TOF distributions, the trapping desorption component appears to be enhanced relative to the direct inelastic component because 1) there is an untrue enhancement of the signal at long times due to inelastic scattering of thermalized O atoms and O_2 molecules that effuse out of the source chamber through the skimmer, and 2) species traveling more slowly through the ionizer have a greater probability of being ionized than faster species (the flux $I(t)$ is proportional to $N(t)/t$). Therefore, we estimate that the trapping desorption component is less than 20% for both O and O_2 inelastic scattering. It is important to note that the relative fraction of trapping desorption may vary considerably depending on the initial and final scattering angles.[11] The average fractional energy transfer for direct inelastic scattering is also dependent on the initial and final scattering angles. Surface roughness may reduce the fraction of direct inelastic scattering; however, we have observed large direct inelastic scattering components in our laboratory even when O-atoms scatter from the very rough surface of a graphite polysulfone composite material. Finally, for comparison we note that an earlier surface energy accommodation study[12] with roughly 5 eV O atoms impinging on metal and glass surfaces implied a significant amount of direct inelastic scattering with the reported energy accommodation coefficients of approximately $0.6 \pm 50\%$.

Figure 8 shows TOF distributions of carbon dioxide products emerging from the surfaces of Kapton HN and ^{13}C-enriched Kapton after being struck by the hyperthermal beam pulse. Again, time zero corresponds to the firing of the laser. On the left is signal from Kapton HN, and on the right is signal from ^{13}C-enriched Kapton. As can be seen, the $^{12}CO_2$ signal from plain Kapton is distributed between $^{12}CO_2$ and $^{13}CO_2$ when the reaction occurs with ^{13}C-enriched Kapton. The fact that the sum of the signals at the two isotopes from ^{13}C-enriched Kapton add up to the signal at the one isotope from plain Kapton HN indicates that the signals must originate from reactions with the actual sample materials and not contamination on them.

Two key observations stand out in the carbon dioxide TOF distributions. First, the $^{12}CO_2$ signal from ^{13}C-enriched Kapton is higher than the $^{13}CO_2$ signal even though there are more C-13 carbons in the polymer chain. This observation suggests that volatile CO_2 is coming preferentially from reactions with the imide component of the polymer repeat unit. Second, there are two components in the TOF distributions. It is clear from the bimodal distributions that two kinds of interactions lead to CO_2 products. The faster signal corresponds to products that are ejected from the surface at hyperthermal energies ($\sim$0.7 eV), and the slower signal corresponds to reaction products that leave the surface at velocities given by the surface temperature. The fast products may come from a direct reaction (Eley-Rideal mechanism[13]) on the surface with carbonyl groups that are part of the polyimide polymer or that accumulate on the surface during O-atom bombardment, or perhaps CO_2 residing on the surface is knocked off by collision-induced desorption. The slow products, on the other hand, are probably the result of a surface reaction that follows initial adsorption of the impinging O atoms on the surface (Langmuir-Hinshelwood mechanism[13]).

We see an analogous behavior for the CO reactive products (Fig. 9). The signal is generally lower, and the relative magnitude of the hyperthermal component is larger.

Figure 10 shows TOF distributions collected at two other product masses, corresponding to H_2O and NO. As expected, there is not much difference between the two forms of Kapton at these unlabeled masses. The shape of the NO^+ TOF distribution is uncertain because the raw data contained a relatively large contribution from inelastic scattering of O_2, which could still be detected at $m/z = 30$ with the mass spectrometer resolution employed. We therefore estimated the contribution from O_2 to the $m/z = 30$ TOF distribution and subtracted it to arrive at the distribution shown in Fig. 10.

These preliminary data show some interesting features that suggest preferential attack at the imide group in the polymer and two types of interaction mechanisms with the surface, giving rise to thermal and hyperthermal products. A complete understanding of these data will require a detailed study of the TOF distributions at many masses as a function of incident angle, final angle, surface temperature, incident energy, and incident species. For example, the hyperthermal, or direct-reaction, signal may depend strongly on incident energy and exit angle and only weakly on surface temperature, whereas the thermal, or indirect-reaction signal may have a cosine angular distribution regardless of incident kinetic energy, and only a change in surface temperature would affect arrival time.

The observation of more CO and CO_2 products from reaction with the imide component of the polymer raises questions about the fate of the ether component. It appears from our data that the ether component may degrade partly through release of volatile species other than CO or CO_2. If these volatile species are higher-molecular-weight hydrocarbon fragments, then they could pose a contamination threat on a spacecraft. Future experiments should include a careful search over a wide mass range in order to identify any heavier volatile products that might be evaporating from the surface.

COMPARISON OF LAB AND SPACE RESULTS

The laboratory TOF distributions can be integrated to arrive at a mass spectrum that can be compared with the EOIM-3 carousel mass spectrum from ^{13}C-enriched Kapton. Figure 11 shows two representations of the flight data with the laboratory mass spectrum in the middle. There are four peaks in the flight mass spectrum that can be compared with our laboratory mass spectrum of reactive products: m/z = 29($^{13}CO^+$), 30(NO^+), 44($^{12}CO_2^+$), and 45($^{13}CO_2^+$). The water peak (m/z = 18) is too large and variable in the flight data to be meaningful, and the m/z = 28 peak in the flight data is dominated by N_2, which is in the ambient LEO environment.

The lab data show more $^{12}CO_2$ than $^{13}CO_2$, and the same may be true in the space data. The main difference between the lab and flight data is the relatively high ratio of $^{13}CO_2$ to ^{13}CO products in the lab as compared with space. The apparently high CO_2 signal in the lab might arise from the high O_2 component in the hyperthermal beam (the fraction of O_2 in the EOIM-3 environment is $<5\%$). Perhaps O_2 adds to radical sites on the surface and/or dissociates on impact, leading to O-atom reactions on the surface. In either case, the level of surface oxidation would increase and thus favor the more highly oxidized form of carbon, i.e., CO_2.

Although the lab and flight results are preliminary, they do appear similar. Further laboratory studies with a beam much reduced in molecular oxygen may show even better agreement with the space data. It is important to have a common point of agreement between the lab and flight experiments in order to lend credence to the laboratory experiments as representative of the interactions that take place in LEO. Our laboratory experiment is much more sophisticated than the EOIM-3 carousel experiment and can therefore reveal much more about the interaction mechanisms of hyperthermal O atoms with Kapton (or any other material); however, the value of these and future lab results to the space environment and effects community will ultimately be judged by their "calibration" with space experiments.

ACKNOWLEDGEMENTS

The research described in this report was carried out by the Jet Propulsion Laboratory, California Institute of Technology, under contract with the National Aeronautics and Space Administration (NASA). The sponsoring NASA agency was the Materials and Structures Division, Office of Aeronautics and Exploration Technologies. Partial support was also provided by the Space Environmental Effects Program of the Ballistic Missile Defense Organization (BMDO) Innovative Science and Technology Directorate. The authors wish to thank Dr. David Brinza, who conceived and planned the EOIM-3 carousel experiment with the isotopically-labeled Kapton, and Dr. Andre Yavrouian for synthesizing the ^{13}C-enriched Kapton. The assistance of Dr. Mark Hanning-Lee in obtaining the space data presented here is also appreciated.

REFERENCES

1. Minton, T. K.: Protocol for Atomic Oxygen Testing of Materials in Ground-Based Facilities; Version Number 1. JPL Publication 94-02, April 1, 1994.

2. Chung, S. Y.; Brinza, D. E.; Minton, T. K.; Stiegman, A. E.; Kenny, J. K.; and Liang, R. H.: Flight- and Ground-Test Correlation Study of BMDO SDS Materials; Phase I Report. JPL Publication 93-31, December 1993.

3. Lee, Y. T.; McDonald, J. D.; LeBreton, P. R.; and Herschbach, D. R.: Molecular Beam Reactive Scattering Apparatus with Electron Bombardment Detector. Rev. Sci. Instrum. **40**, 1402 (1969).

4. Brinza, D. E.; Coulter, D. R.; Chung, S. Y.; Smith, K. O.; Moacanin, J.; and Liang, R. H.: A Facility for Studies of Atomic Oxygen Interactions with Materials. Proceedings of the 3rd International SAMPE Electronics Conference, p. 646 (1989).

5. Caledonia, G. E.; Krech, R. H.; and Green, B. D.: A High Flux Source of Energetic Oxygen Atoms for Material Degradation Studies. AIAA J. **25**, 59 (1987).

6. Proch, D. and Trickl, T.: A High-Intensity Multi-Purpose Piezoelectric Pulsed Molecular Beam Source. Rev. Sci. Instrum. **60**, 713 (1989).

7. Rettner, C. T. and Ashfold, M. N. R.: Dynamics of Gas-Surface Interactions; Advances in Gas-Phase Photochemistry and Kinetics Series. (Royal Society of Chemistry, Cambridge, 1991).

8. Rettner, C. T.; Schweizer, E. K.; and Mullins, C. B.: Desorption and Trapping of Argon at a 2H-W(100) Surface and a Test of the Applicability of Detailed Balance to a Nonequilibrium System. J. Chem. Phys. **90**, 3800 (1989).

9. Rettner, C. T.; Barker, J. A.; and Bethune, D. S.: Angular and Velocity Distribution Characteristic of the Transition between the Thermal and Structure Regimes of Gas-Surface Scattering. Phys. Rev. Lett. **67**, 2183 (1991).

10. Saecker, M. E.; Govoni, S. T.; Kowalski, D. V.; King, M. E.; and Nathanson, G. M.: Molecular Beam Scattering from Liquid Surfaces. Science **252**, 1421 (1991).

11. King, M. E.; Nathanson, G. M.; Hanning-Lee, M. A.; and Minton, T. K.: Probing the Microscopic Corrugation of Liquid Surfaces with Gas-Liquid Collisions. Phys. Rev. Lett. **70**, 1026 (1993).

12. Krech, R. H.; Gauthier, M. J.; and Caledonia, G. E.: High Velocity Atomic Oxygen/Surface Accommodation Studies. J. Spacecraft and Rockets **30**, 509 (1993).

13. Atkins, P. W.: Physical Chemistry (Freeman, New York, 1986) 3rd ed., pp. 782-3.

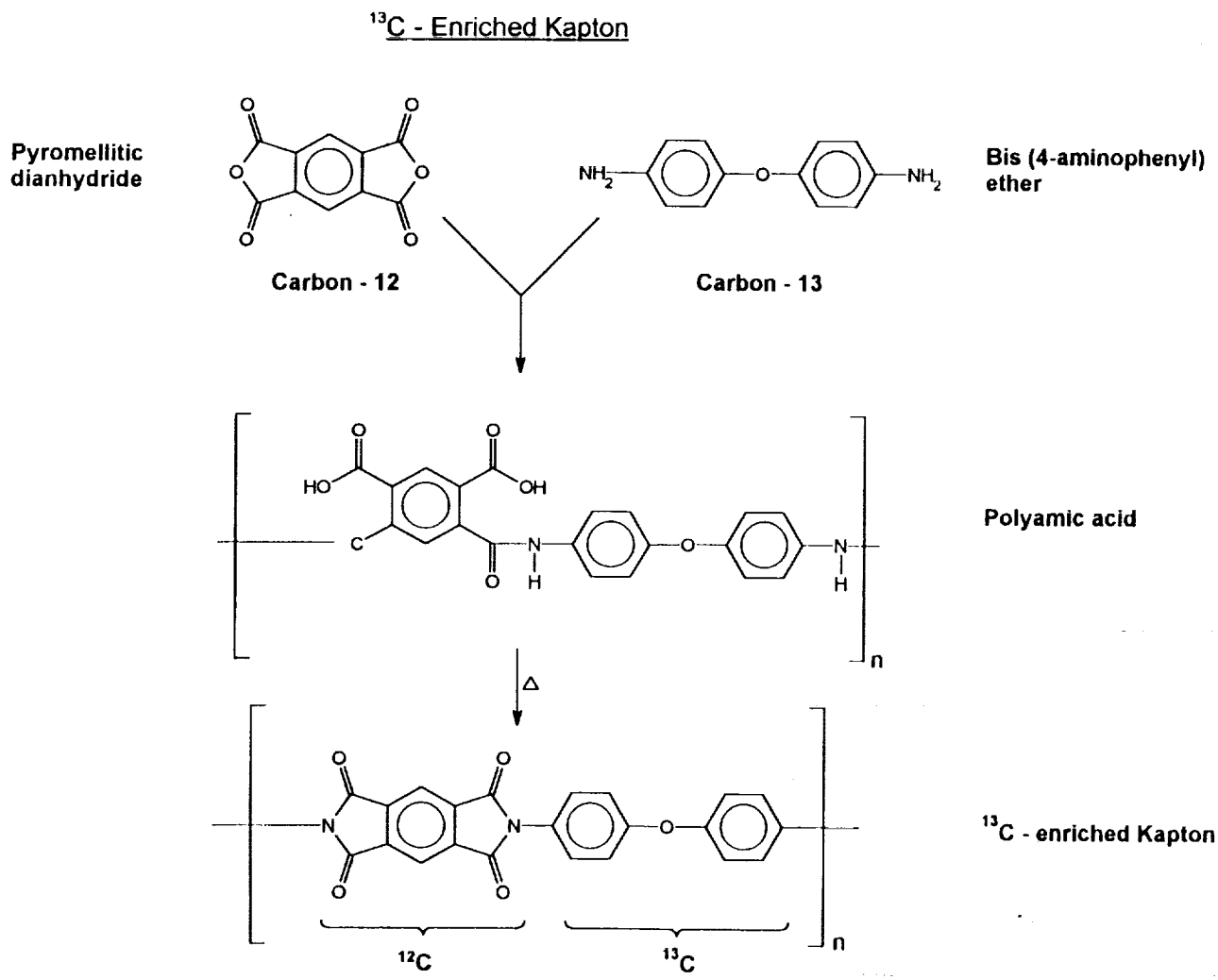

Figure 1. Key steps in the synthesis of ^{13}C-enriched "Kapton."

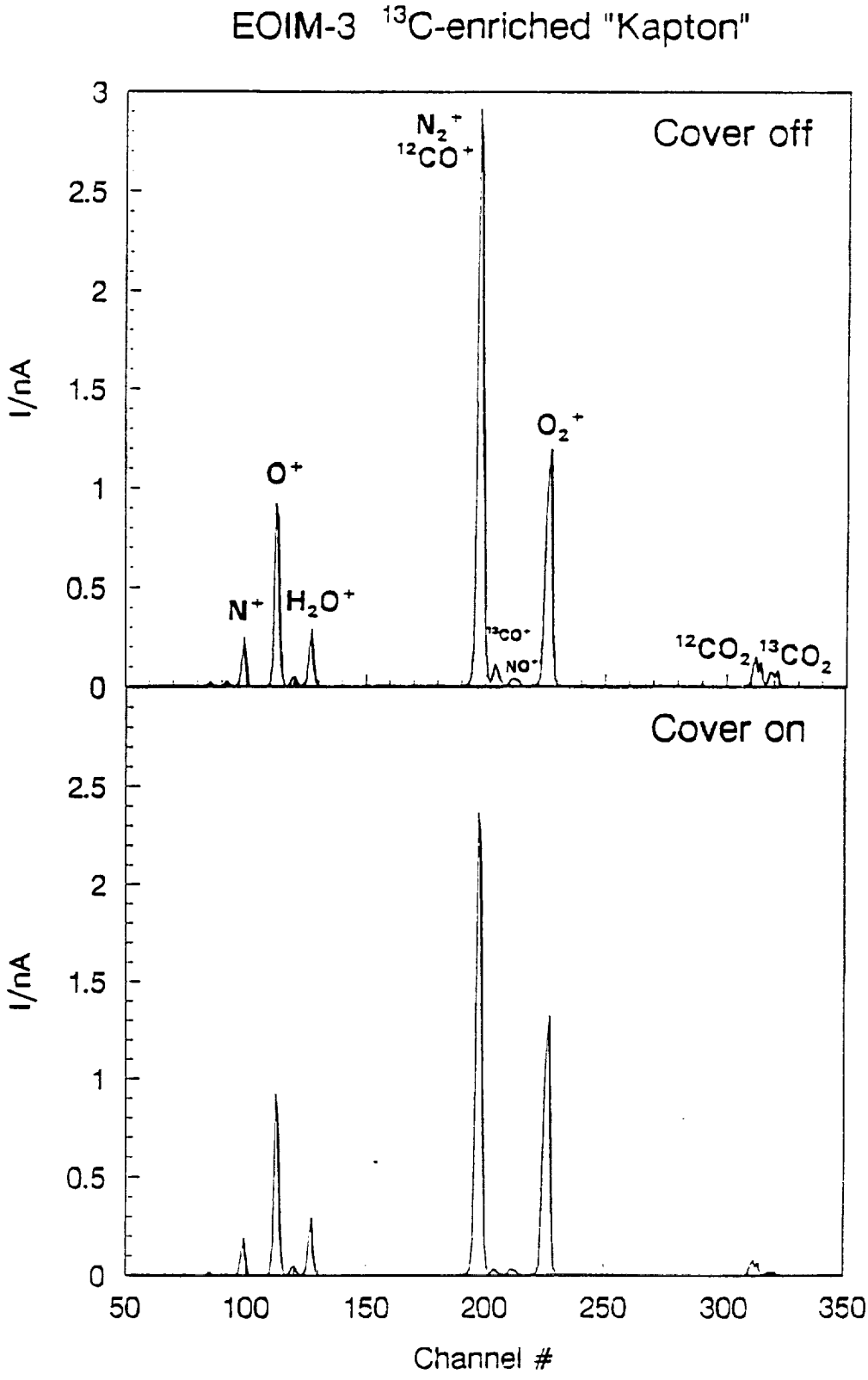

Figure 2. Mass spectra taken with EOIM-3 mass spectrometer viewing ^{13}C-enriched Kapton on the carousel.

JPL Crossed Molecular Beams Apparatus

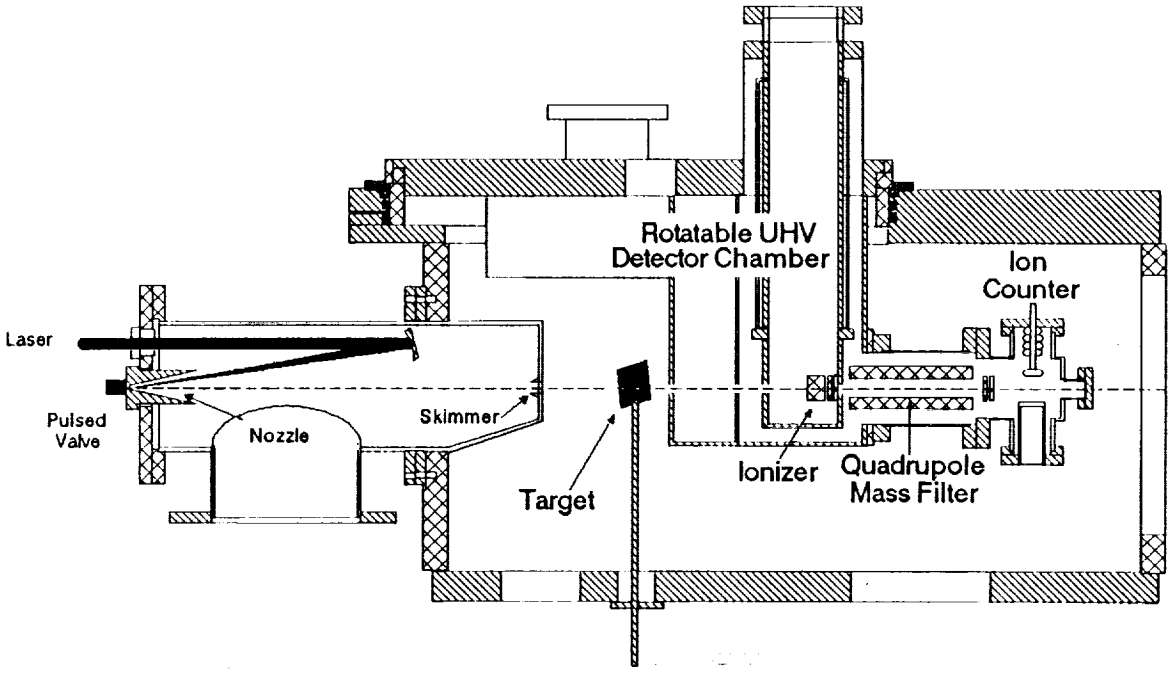

Hyperthermal Beam – Surface Studies

Figure 3. Schematic diagram of molecular beam apparatus.

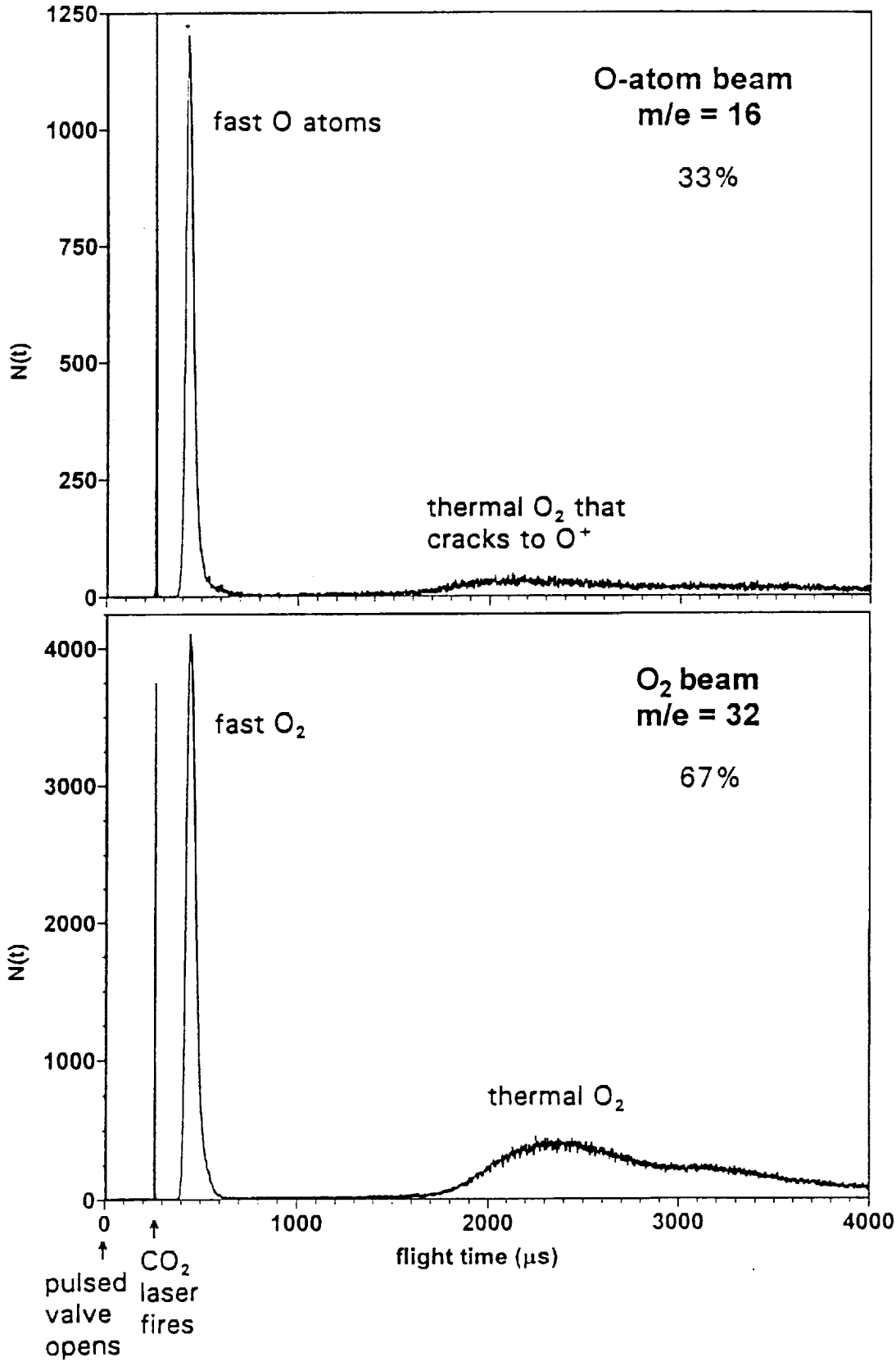

Figure 4. Time-of-flight distributions of the molecular beam collected at two masses.

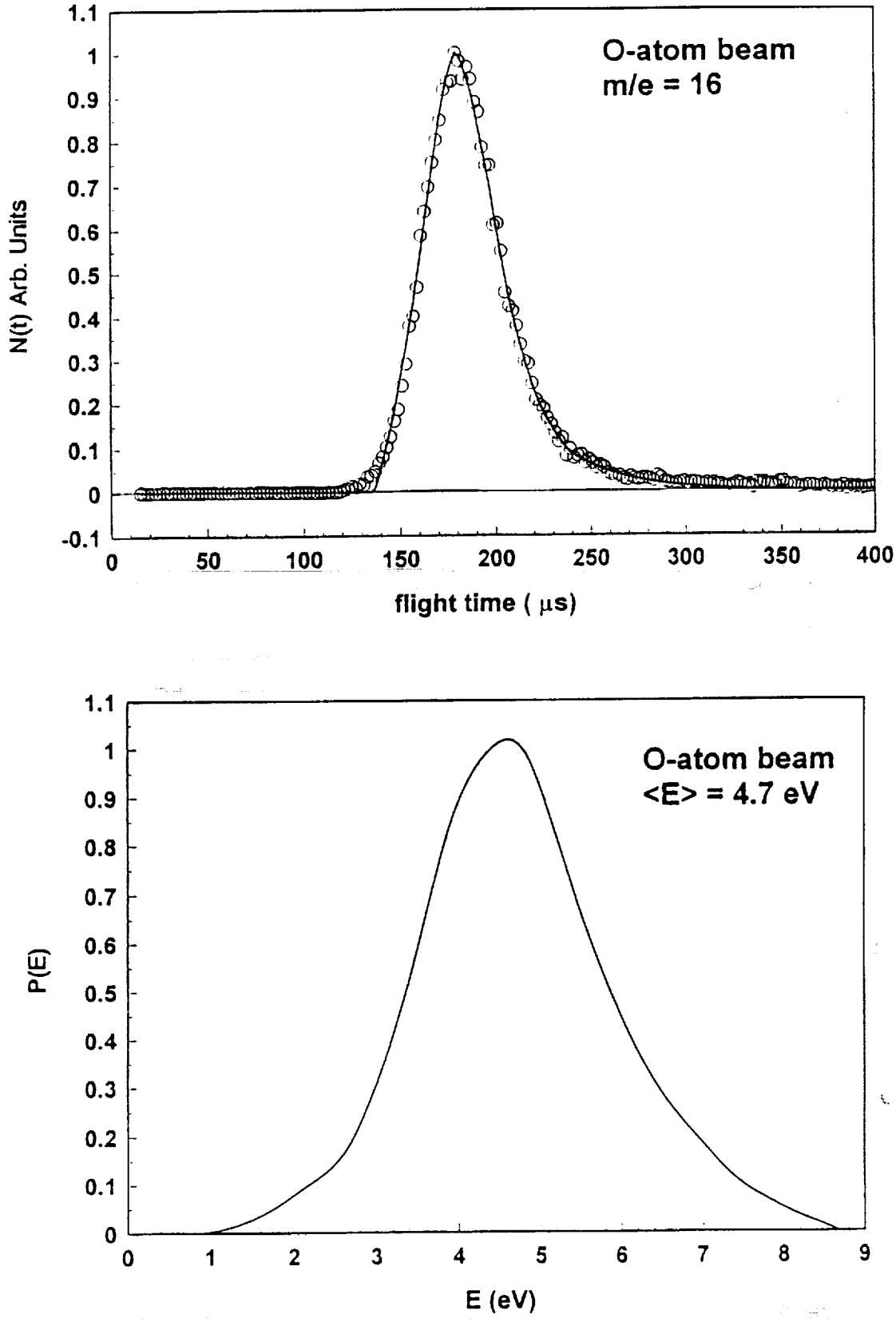

Figure 5. Time-of-flight and translational energy distributions of the O-atom component in the molecular beam.

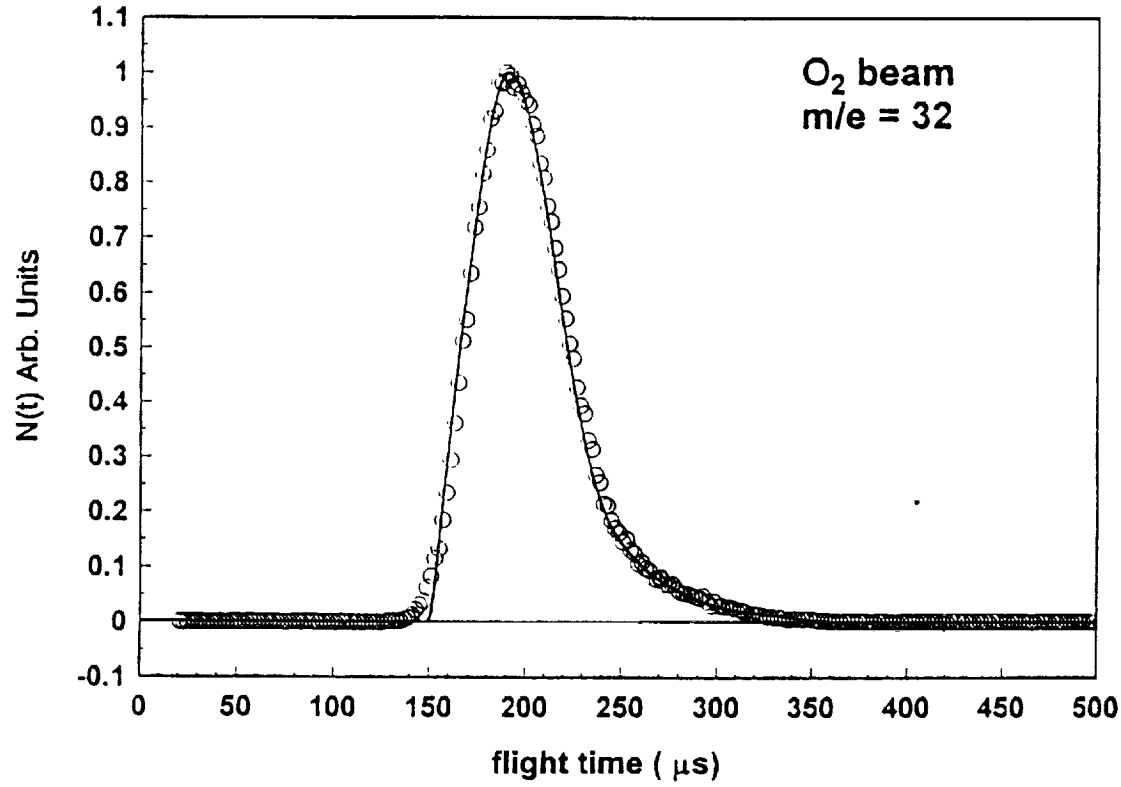

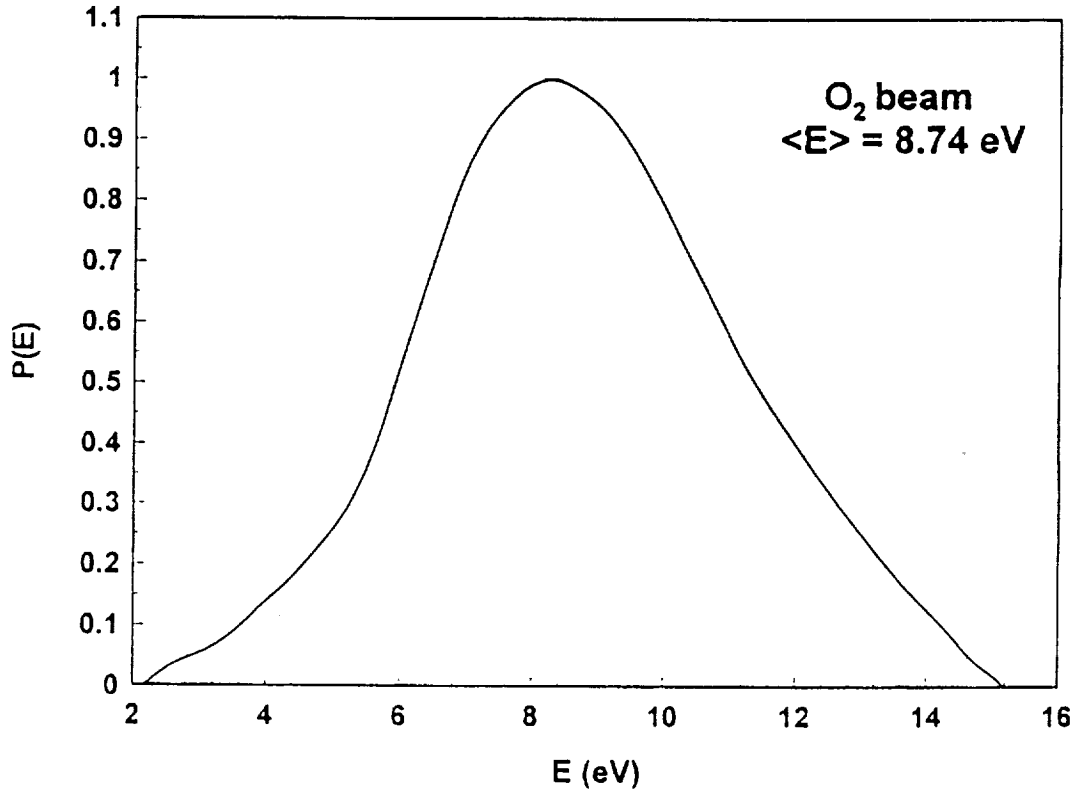

Figure 6. Time-of-flight and translational energy distributions of the fast O_2 component in the molecular beam.

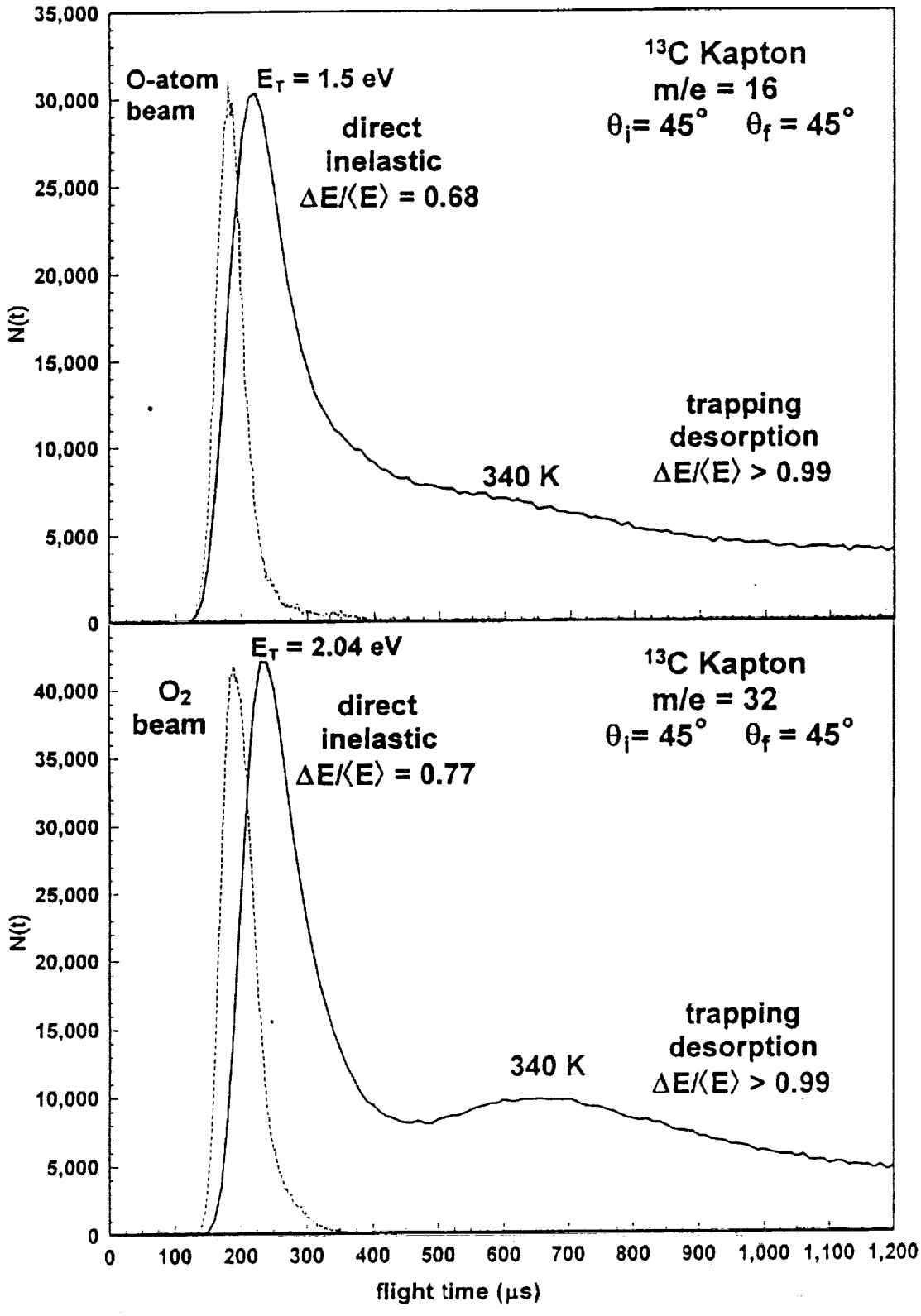

Figure 7. Time-of-flight distributions of O and O_2 scattered from a ^{13}C-enriched Kapton surface.

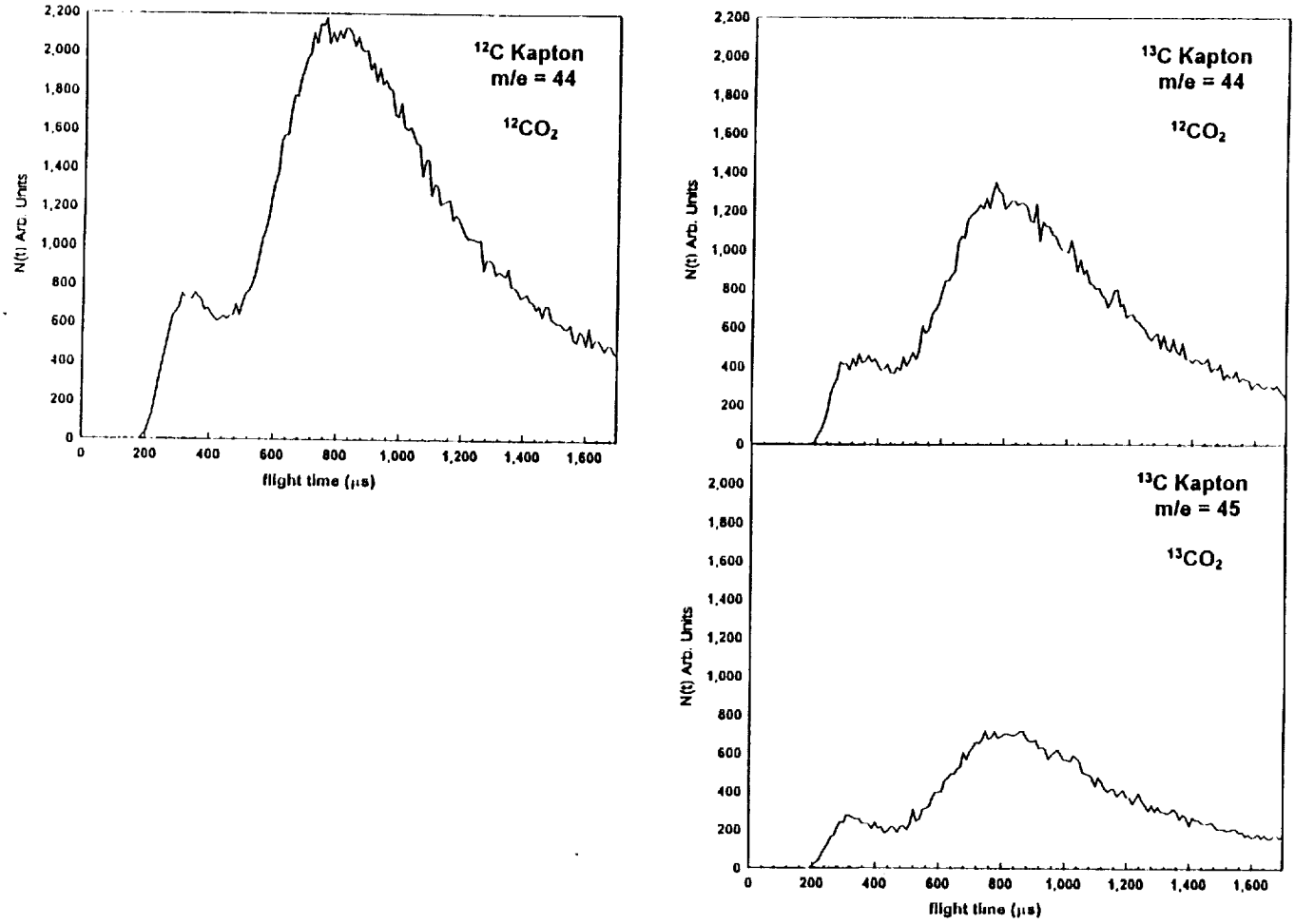

Figure 8. Time-of-flight distributions of CO_2 products emerging from Kapton HN (^{12}C Kapton) and ^{13}C-enriched Kapton surfaces.

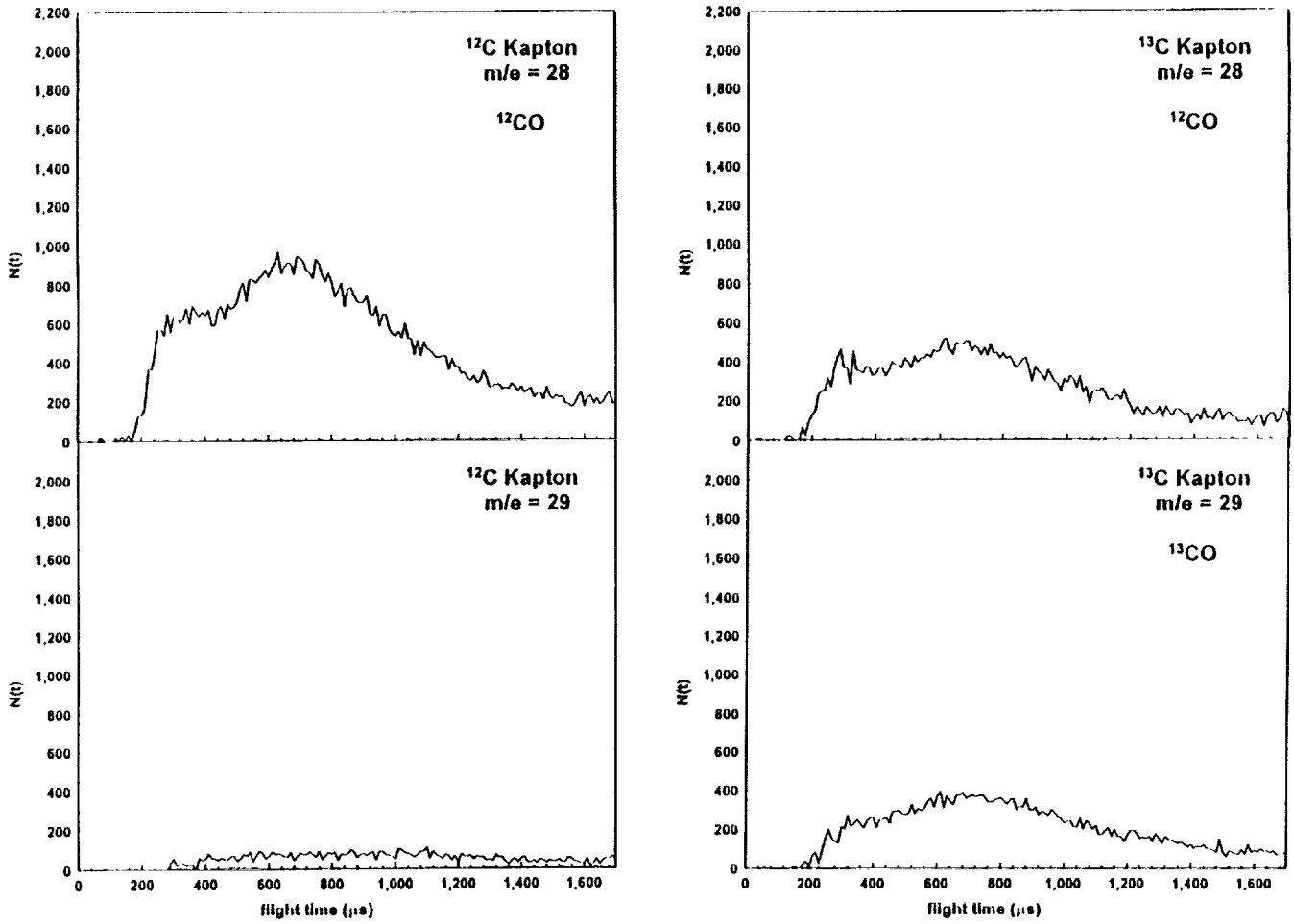

Figure 9. Time-of-flight distributions of CO products emerging from Kapton HN (^{12}C Kapton) and ^{13}C-enriched Kapton surfaces.

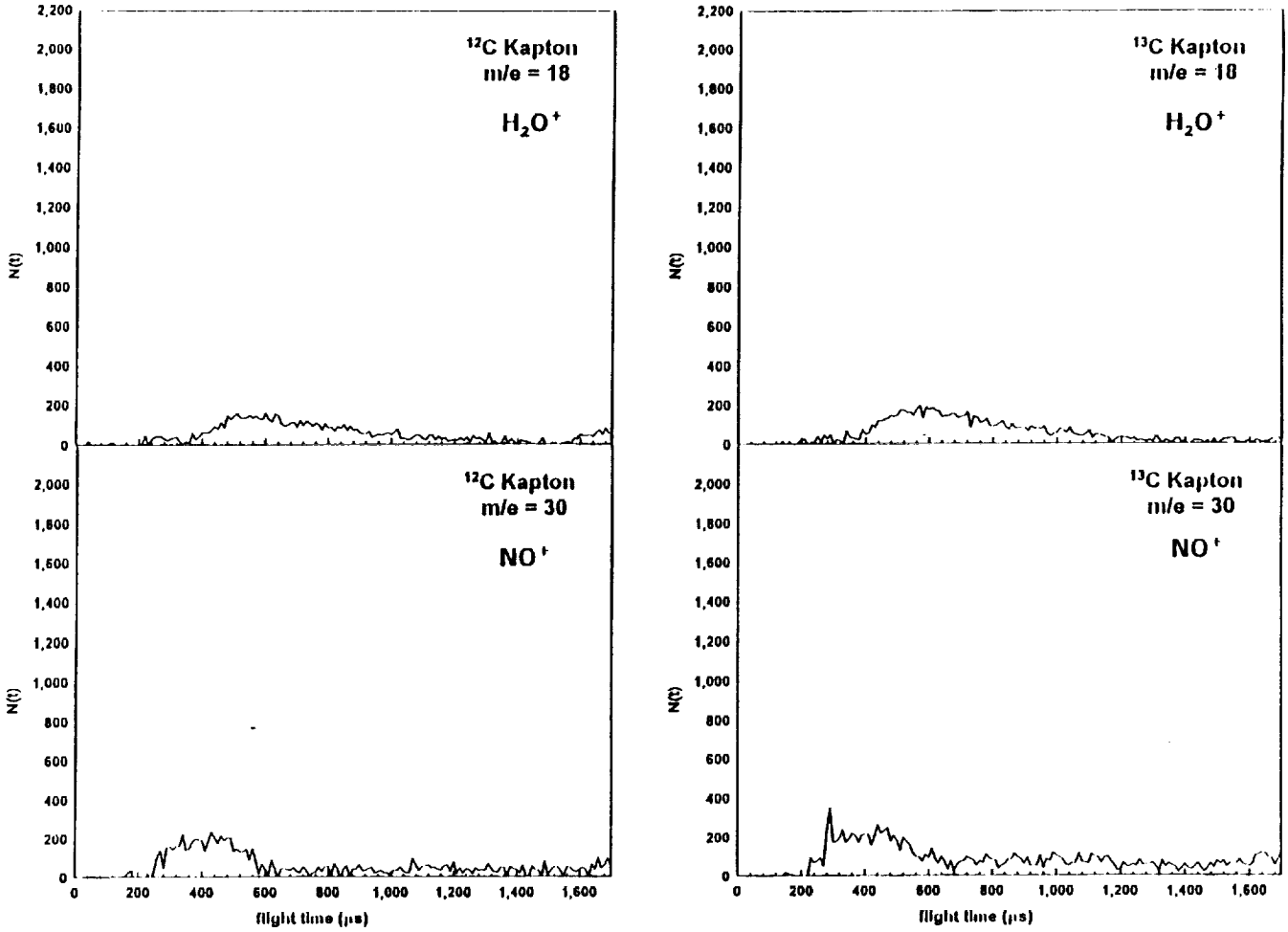

Figure 10. Time-of-flight distributions of H_2O and NO products emerging from Kapton HN (^{12}C Kapton) and ^{13}C-enriched Kapton surfaces.

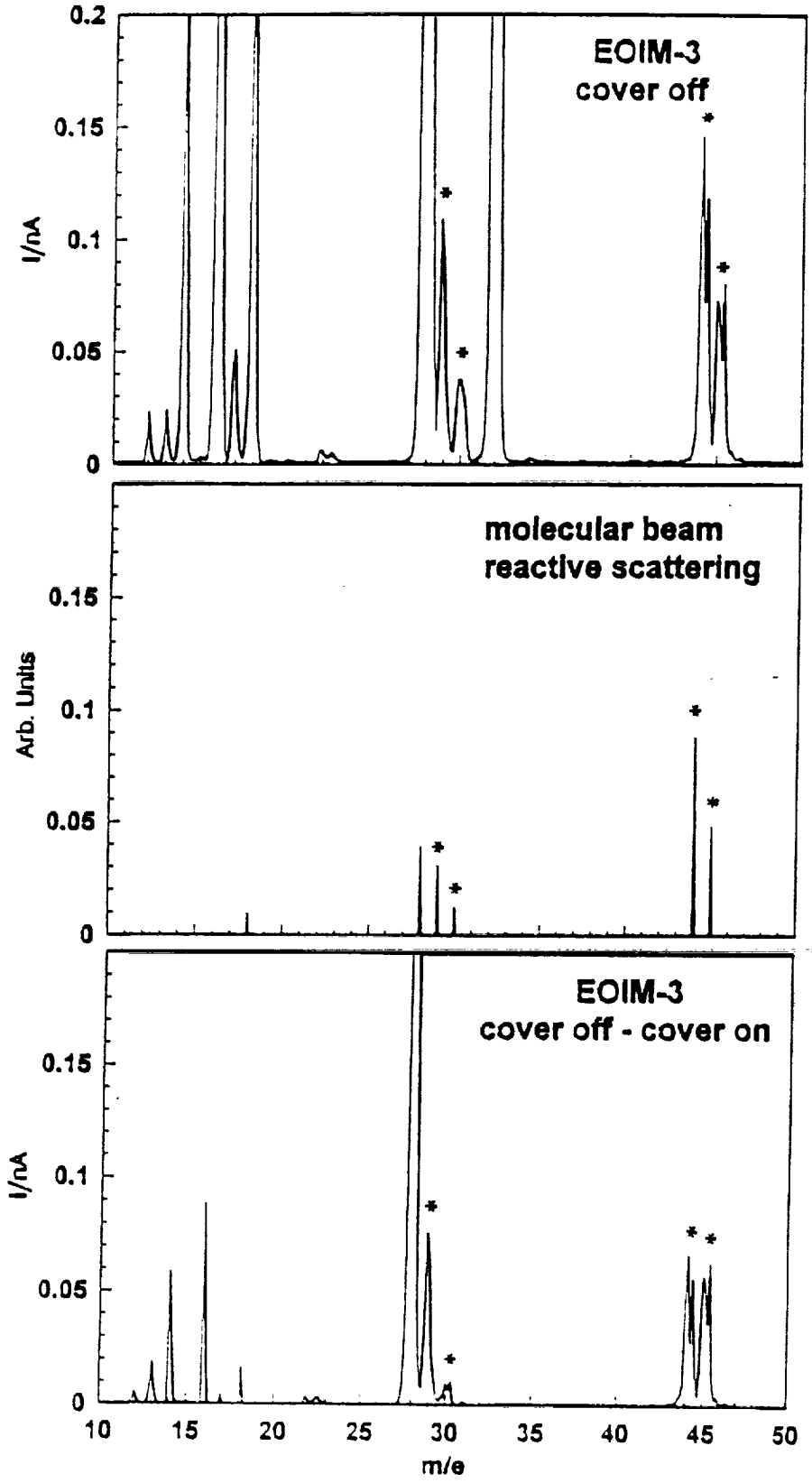

Figure 11. Comparison of mass spectra collected in space (top and bottom panels) and in the laboratory (center panel).